Ratchet Transport and Periodic Structures in Parameter Space

A. Celestino,[1] C. Manchein,[1,2] H. A. Albuquerque,[1] and M. W. Beims[2]
[1]Departamento de Física, Universidade do Estado de Santa Catarina, 89219-710 Joinville, Brazil
[2]Departamento de Física, Universidade Federal do Paraná, 81531-980 Curitiba, Brazil
(Received 5 February 2011; published 6 June 2011)

This work analyzes the parameter space of a discrete ratchet model and gives direct connections between chaotic domains and a family of isoperiodic stable structures with the ratchet current. The isoperiodic structures, where larger currents are usually observed inside, appear along preferred direction in the parameter space giving a guide to follow the current. Currents in parameter space provide a direct measure of the momentum asymmetry of the multistable and chaotic attractors times the size of the corresponding basin of attraction. Transport structures are shown to exist in the parameter space of the Langevin equation with an external oscillating force.

DOI: 10.1103/PhysRevLett.106.234101 PACS numbers: 05.45.Ac, 05.45.Pq

The description of the ratchet transport of particles in nature has become an actual and largely studied problem due to the possibility of obtaining transport properties without external bias. Intuitively such transport is due to the rectification of an external net-zero force to obtain directional motion of particles in spatially periodic media. To obtain ratchet transport, spatiotemporal symmetries must be broken in the system [1]. Ratchets have become natural candidates for describing transport phenomena in Brownian [2,3] and molecular motors [4], cold atoms [5], migration of bacteria [6], cell mobility in cancer metastasis [7], granular gas [8], fluid transport [9], and in more general areas like classical and quantum physics [10], chemistry [11] and biophysics [12]. These are just some references in the distinct areas, since the actual literature related to ratchets is enormous.

A common feature of interest in all areas of ratchets applications is the understanding, achievement, and control of transport. *A priori*, dynamical variables and parameters of the system (like temperature, dissipation, noise intensity, external forces, etc.), which control the dynamics, are deeply interconnected so that it is very hard to make general statements about the ratchet current (RC) as a function of the parameters. The precise determination of the nature of transport in unbounded systems is still not fully understood; thus, it is very desirable to achieve and/or recognize ''patterns'' or ''structures'' in the parameter space which are directly connected to transport properties. Is it even more attractive if such transport structures present universal features observed in a large class of dynamical systems.

This Letter analyzes the parameter space of a ratchet model and shows the relation between ratchet currents with a family of isoperiodic stable structures (ISSs) and chaotic domains in parameter space. A remarkable complete connection between parameters of the system and the RC is given, and therefore general clues for the origin of directed transport. To mention an example, one of the ISSs observed here, which has a shrimp-shaped form [see Fig. 3(c)], has already appeared in the parameter space of generic dynamical systems and applications. Such shrimps were found to be generic structures in the parameter space of dissipative systems like maps [13,14] and continuous models [15], among others. Very recently they were also observed in experiments with electronic circuits [16]. We show here that such shrimp-shaped structures are also essential to directed transport in nature. As for shrimps [13], the ISSs described here are Lyapunov stable islands with dynamics globally structurally stable.

In order to show generic properties of the RC in the parameter space, we use a map M which presents all essential features regarding unbiased current [17]

$$M:\begin{cases} p_{n+1} = \gamma p_n + K[\sin(x_n) + a\sin(2x_n + \phi)], \\ x_{n+1} = x_n + p_{n+1}, \end{cases} \quad (1)$$

where p_n is the momentum variable conjugated to x_n, $n = 1, 2, \ldots, N$ represents the discrete time and K is the nonlinearity parameter. The dissipation parameter γ reaches the overdamping limit for $\gamma = 0$ and the conservative limit for $\gamma = 1$. The ratchet effect appears due to the spatial asymmetry, which occurs with $a \neq 0$ and $\phi \neq m\pi$ ($m = 1, 2, \ldots$), in addition to the time reversal asymmetry for $\gamma \neq 1$. The RC of the above model was studied [17] for fixed $K = 6.5$ in the dissipation interval $0 \leq \gamma < 1$.

Figure 1 shows the RC $= \frac{1}{M}\sum_{j=1}^{M}[\frac{1}{N}\sum_{n=1}^{N} p_n^{(j)}]$ (colors) as a function of the dissipation parameter γ and the nonlinearity parameter K, where M is the number of initial conditions. A remarkable complex structure of colors is evident, where each color is related to a given value of the current (see color bar). Black colors are related to close to zero currents; green to white colors (gray to white in the gray scale) are related to increasing positive currents while red to yellow colors (gray to white in the gray scale) related to increasing negative currents. The white straight line at $K = 6.5$ corresponds to the case analyzed recently [17]. Three main regions with distinct behaviors can be

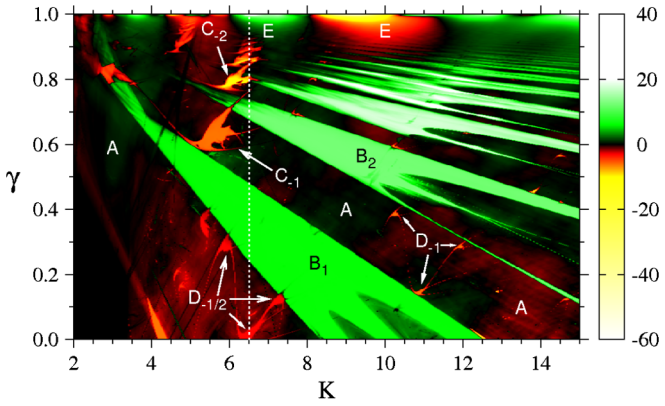

FIG. 1 (color online). The RC (see color bar) plotted in the parameter space (γ, K) with a grid of 600×600 points, $a = 0.5$, $\phi = \pi/2$, 10^5 initial conditions with $\langle p_0 \rangle = \langle x_0 \rangle = 0$ inside the unit cell $(-2\pi, 2\pi)$, and $N = 10^4$ iterations.

identified: (i) a large "cloudy" background, identified as A in Fig. 1, mixed with black, red, and green colors (black, gray to light gray), showing a mixture of zero, small negative and positive currents, respectively; (ii) several structures with sharp borders (the ISSs) and distinct colors, which are embedded in the cloudy background region and are identified in Fig. 1 as B_L, C_L, and D_L (L is an integer or rational number); (iii) strong positive and negative currents (region E), with not well defined borders which occur close to the conservative limit $\gamma = 1$. Next we explain in more detail these distinct regions by analyzing other quantities.

Figure 2 shows the parameter space (γ, K) for the period q from the orbits. Periodic stable motion is restricted to well-defined structures while the black background is related to the chaotic motion. This was checked by determining (not shown) the parameter space for the largest Lyapunov exponent (LE). Zero and negative LEs

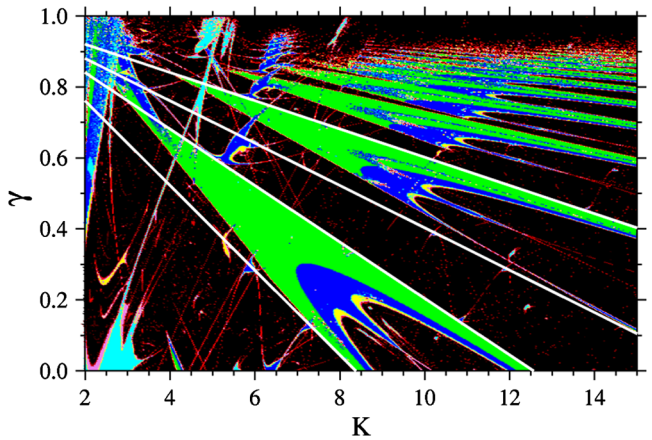

FIG. 2 (color online). Period-q values in parameter space (γ, K): green (gray): $q = 1$, blue (dark gray): $q = 2$, cyan (light gray): $q = 3$, yellow (white): $q = 4$, red (isolated white points) $8 \leq q \leq 12$, and black for no period. In this case only one initial condition is used ($x_0 = 0.5$, $p_0 = 0.3$), $N = 10^6$ iterations and a grid of 600×600 points.

are related to the periodic motion and positive LEs to the black regions of Fig. 2. This already allows us to associate the cloudy region A from Fig. 1 with the chaotic motion. Thus the small portions of negative or positive currents [red and green (gray) clouds] are due to the chaotic transport, consequence of the asymmetry of the chaotic attractor [5].

Map (1) is periodic in x with period 2π. Thus the condition for a period-q orbit is $\sum_{i=n}^{n+q-1} p_i = 2\pi m$, with integer $m = \ldots, -2, -1, 0, 1, 2, \ldots$ which represent the net number of left (negative) or right (positive) 2π jumps in x over the period. The mean momentum for a given period q is then $\bar{p}_q = \sum_{i=n}^{n+q-1} p_i/q = 2\pi m/q$ which can be written as $2\pi L$, so that $L = m/q$. Therefore L, which gives $\bar{p}_q$ in units of 2π, can assume fractional values (positive or negative). All ISSs from Fig. 1 coincide with the sharp borders of Fig. 2 and a direct connection between periodic stable motion and the RC is given. Regarding these sharp structures we observe three different ISSs: B_L composed by the sequence $L = 1, 2, \ldots$ of dominant diagonal structures with main period $q = 1$ [see green (gray) main regions in Fig. 2] which extend themselves along a large range of K values. As K increases and γ decreases, inside each structure B_L we observe 1×2^n [green (gray) $\rightarrow$ blue (dark gray) $\rightarrow$ yellow (white) $\rightarrow \ldots$] doubling cascades bifurcations. Comparing to Fig. 1, we observe that the current inside each structure B_L is independent of the period q and thus, on the bifurcation points. At the doubling bifurcation cascades 1×2^n we observed that $m \rightarrow 2m$ so that L $(= m/q = \bar{p}_q/2\pi)$ remains constant inside each structure B_L. Even though different isoperiodic B_L structures have the same period, RCs increase with L and γ. Structures B_L are very similar to the cuspidal singularities [18]. Since the boundary of structures B_L are born at period $q = 1$, they can be calculated analytically from the eigenvalues of the Jacobian of the map (1) after one iteration. Using $\phi = \pi/2$, the fixed points from (1) can be calculated from $p^{(1)} = 2\pi L$ (L integer) and $2\pi L(\gamma - 1) + K[\sin(x^{(1)}) + a\cos(2x^{(1)})] = 0$. The solutions are $x_j^{(1)} = \arctan(\alpha^{(-)}, \pm\beta^{(+)})$ $(j = 1, 2)$ and $x_s^{(1)} = \arctan(\alpha^{(+)}, \pm\beta^{(-)})$ $(s = 3, 4)$ where $\alpha^{(\mp)} = \mp\sqrt{K[3K + 8L\pi(\gamma - 1)]} + K$ and $\beta^{(\pm)} = \sqrt{8KL\pi(1-\gamma) \pm 2\sqrt{K^2[3K + 8L\pi(\gamma - 1)]}}$. Substituting these solutions in the Jacobian of the map (1) we obtain analytical expressions $\lambda(\gamma, K, L)$ for the two eigenvalues. When $\lambda(\gamma, K, L) = +1$ (born of period 1), we obtain a relation between γ, K, and L where period-1 orbits are born in parameter space. The solutions for $\lambda(\gamma, K, L) - 1 = 0$, for all fixed points $x_j^{(1)}$, are $\gamma_1^{(L)} = 1 - 3K/(8\pi L)$ (lower border) and $\gamma_2^{(L)} = 1 - K/(4\pi L)$ (upper border). Both curves define exactly, for a given L, the sharp period-1 B_L boundaries of Figs. 1 and 2. The border of the first large dominant structure B_1 is obtained from $L = 1$, the

second one B_2 from $L = 2$, and so on. See white lines $\gamma_1^{(L=1)}$, $\gamma_2^{(L=1)}$, $\gamma_1^{(L=2)}$, and $\gamma_2^{(L=2)}$ in Fig. 2. However, lower borders $\gamma_2^{(L)}$ do not match exactly with the simulations since the basin of attraction related to $q = 1$ is too small compared to the chaotic one and the corresponding current is not observed. This is also exactly what is observed in Fig. 3 from [17], where the left limits of the L intervals are inside the chaotic region. Such analytical description of the boundaries of B_L was obtained from expressions for the eigenvalues in terms of the orbital points. Unfortunately for higher periods (C_L and D_L ISSs below) such expressions are not easy to obtain (if even possible).

The second kind of relevant ISSs, C_L, can be visualized in Fig. 1 close to $K = 6.0$ and $\gamma > 0.5$. They also are ordered in a sequence of structures $L = -1, -2, \ldots$ which approach each other as γ increases, defining a direction in the parameter space obtained by the straight line $\gamma = 0.2845K - 0.994\,925$, along which negative currents increase [see dashed line in Fig. 3(a)]. The main period of each C_L is $q = 2$ (blue, dark gray) [Fig. 3(b)] but, inside each structure, period-doubling cascades bifurcations appear when going to the border of the structures, where the chaotic region is reached. For clarity Figs. 3(a) and 3(b) present the current and period as a magnification for these structures. Again we observe that current increases (in modulus) along the sequences as γ increases.

The last observed ISSs, D_L, appear embedded in the cloudy chaotic background and present the well-known shrimp-shaped form. For example, three connected structures (D_{-1}) appear in the interval $10 < K < 12$ and

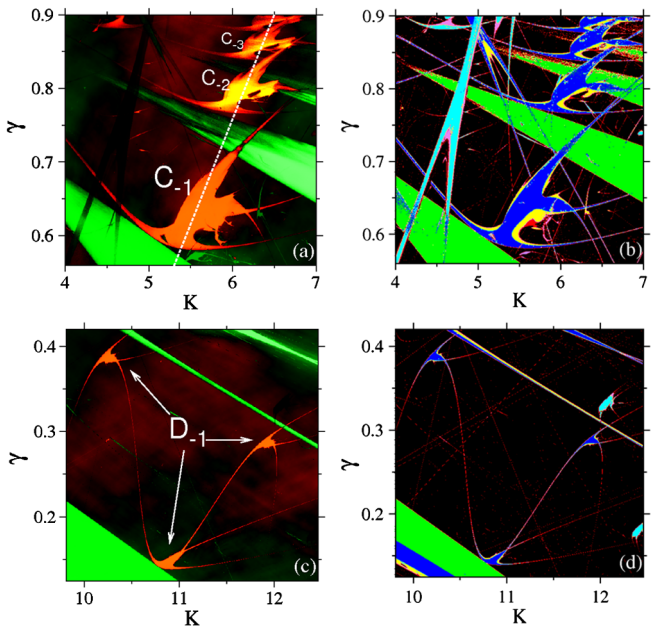

FIG. 3 (color online). Magnifications of Fig. 1 (left) and Fig. 2 (right) showing that the ISSs are abundant inside the chaotic region and usually organized along specific lines and sometimes connected to each other.

$0.1 < \gamma < 0.4$ [see also Fig. 3(c)]. Another example is demarked in Fig. 1 by $D_{-1/2}$. These structures have a main body with period $q = 2$ and a succession of domains related to period-doubling route to chaos. They are also distributed in sequences along preferred direction in the parameter space, as can be seen by looking carefully at Fig. 1, where many shrimp-shaped ISSs are hidden behind the dominant B_L structures. Such preferential directions in parameter space appear to be general properties of shrimp-shaped ISSs (see [13]) which are abundant in the parameter space, as shown in the magnifications in Figs. 3(c) and 3(d). As the parameter space is searched further and further for finer domains, a large amount of distinct ISSs appear, usually well organized and sometimes even connected to each other [see the connected shrimp-shaped ISSs in Fig. 3(c)]. Connected ISSs have the same RC.

The region E presents larger currents close to $\gamma = 1$ with not well-defined borders. We start by mentioning that the parameter space for the largest LE (not shown here) in this region is positive and thus totally chaotic. We also clearly see from Figs. 1 and 2 that ISSs with larger L start to overlap each other when $\gamma \to 1$ and thus the number of stable periodic points in phase space increases more and more. Thus a very rich and complex region E is expected, with a mixture of a large number of periodic and chaotic attractors, each one with his own basin of attraction. Such multistability regions were analyzed for the kicked rotor in the beautiful works of [19,20]. It is interesting to observe that apparently the periodic structures are not directly responsible for the currents since large negative RCs are expected at the accumulation of the $C_{-1}, C_{-2} \ldots$ sequence, for example, but current reversal occurs close to $\gamma \to 1$ [see green (gray) region in Fig. 1 at the end of this sequence]. The "competition" between multistable and chaotic attractors in order to generate the RC is gained by the larger basin of attraction of chaotic attractors. Extensive numerical simulations show that close to $\gamma = 1$ the unsharp borders do not change for larger iteration times and that the basins of attraction of periodic orbits are very small compared to the basins of chaotic attractors. This agrees with some recent works [5,17,21] which suggest that the RC in this region is due to the mixture of chaotic motion with tiny island from the conservative case. In fact, accelerator modes from $\gamma = 1$ are responsible for the asymmetry of chaotic attractors, generating the currents. The rich dynamics from regions A, B, C, D, and E from Fig. 1 was also identified for the RC in the parameter spaces (γ, a) and (γ, ϕ) and will be published elsewhere.

In order to show that RCs present generic ISSs in the parameter space of a more general class of dynamical systems, we analyze the zero temperature Langevin equation: $\ddot{x} + \gamma\dot{x} - 5.0[\sin(x) + 0.7\cos(2x)] - K_t \sin(t) = 0$. K_t is the amplitude of the external time oscillating force, γ is the viscosity, and the ratchet potential is identical from Eq. (1).

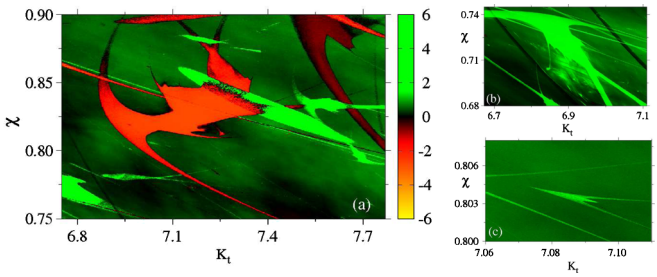

FIG. 4 (color online). ISSs for the RC in the parameter space $(K_t, \chi = e^{(-\gamma)})$ of the Langevin equation.

Figure 4 shows the RC for three distinct regions in the parameter space where some ISSs can be identified: in Fig. 4(b) the green (white) shrimp-shaped; Fig. 4(c) the green (white) cuspidal and Fig. 4(a) the red (gray) C_L which is a mirror reflection of the ISSs from Fig. 3(a). This can also be formally recognized by looking at the corresponding periods in the parameter space (not shown here) and counting the legs that emanate from the structure's main body. Small finite temperatures will slowly transform the sharp borders of the ISSs into unsharp borders and simultaneously enlarge them since their attractors are more stable under noise effects than the chaotic attractors [22].

Concluding, the essential property to obtain finite RCs is the momentum asymmetry of attractors in phase space times the size of the corresponding basin of attraction and can be expressed as $RC = \sum_{i=1}^{N_a} \langle p \rangle_i S_i$, where N_a is the number of attractors, $\langle p \rangle_i$ is the mean momentum of attractor i and S_i is the size (normalized) of attractor i. Thus Figs. 1 and 4 are a direct quantitative measure of RCs which, together with the above expression, allows us to naturally connect to the relevant phase-space dynamics which generates RCs in real systems. We stress that, as much as shrimps and cusps appear in dynamical systems, the isoperiodic stable transport structures B_L (cuspidal shaped), D_L (shrimp shaped) and C_L are generic patterns which should appear in the parameter space of dissipative ratchet system, independent of its application in nature. This was ratified by showing the appearance of the ISSs in the parameter space of the Langevin equation with an external unbiased field. It would be very likely to observe the RCs ISSs in real experiments, as, for example, (a) in the application of a periodic pressure profile in a silicon membrane with asymmetric pores which induces a net motion of the particles from one side of the membrane to the other [23]. Dissipation parameter changes with the liquid viscosity and can be plotted against the pores diameter (nonlinearity K of the ratchet potential) or the pressure amplitude (external amplitude); (b) in the ratchet effect in cold rubidium atoms using the asymmetric optical lattice [24]. Dissipation changes with the Zeeman shift of the ground state and can be plotted against the spatial asymmetry of the potential, which is tailored by changing the magnetic field or the polarizations of counterpropagating waves.

The authors thank CNPq and FINEP (under Project CT-INFRA/UFPR) for partial financial support and G. Benenti and J. A. C. Gallas for discussions.

[1] L. Cavallasca, R. Artuso, and G. Casati, Phys. Rev. E **75**, 066213 (2007).
[2] R. D. Astumian and P. Hänggi, Phys. Today **55**, No. 11, 33 (2002).
[3] P. Reimann, Phys. Rep. **361**, 57 (2002).
[4] F. Jülicher, A. Ajdari, and J. Prost, Rev. Mod. Phys. **69**, 1269 (1997).
[5] G. G. Carlo *et al.*, Phys. Rev. Lett. **94**, 164101 (2005).
[6] G. Lambert, D. Liao, and R. H. Austin, Phys. Rev. Lett. **104**, 168102 (2010).
[7] G. Mahmud *et al.*, Nature Phys. **5**, 606 (2009).
[8] P. Eshuis *et al.*, Phys. Rev. Lett. **104**, 248001 (2010).
[9] K. John, P. Hänggi, and U. Thiele, Soft Matter **4**, 1183 (2008).
[10] S. Kohler, J. Lehmann, and P. Hänggi, Phys. Rep. **406**, 379 (2005).
[11] J. B. Gong and P. Brumer, Annu. Rev. Phys. Chem. **56**, 1 (2005); J. Lehmann *et al.*, J. Chem. Phys. **121**, 2278 (2004).
[12] T. Dittrich and N. Naranjo, Chem. Phys. **375**, 486 (2010).
[13] J. A. C. Gallas, Phys. Rev. Lett. **70**, 2714 (1993).
[14] S. Hayes, C. Grebogi, and E. Ott, Phys. Rev. Lett. **70**, 3031 (1993); M. S. Baptista and I. L. Caldas, Chaos Solitons Fractals **7**, 325 (1996).
[15] C. Bonatto, J. C. Garreau, and J. A. C. Gallas, Phys. Rev. Lett. **95**, 143905 (2005).
[16] R. Stoop, P. Benner, and Y. Uwate, Phys. Rev. Lett. **105**, 074102 (2010).
[17] L. Wang *et al.*, Phys. Rev. Lett. **99**, 244101 (2007).
[18] A. Endler and J. A. C. Gallas, C.R. Acad. Sci. Paris, Ser. I **342**, 681 (2006).
[19] L. C. Martins and J. A. C. Gallas, Int. J. Bifurcation Chaos Appl. Sci. Eng. **18**, 1705 (2008).
[20] U. Feudel *et al.*, Phys. Rev. E **54**, 71 (1996).
[21] S. Denisov *et al.*, Phys. Rev. E **66**, 041104 (2002); H. Schanz *et al.*, Phys. Rev. Lett. **87**, 070601 (2001).
[22] J. A. Blackburn, H. J. T. Smith, and N. Gronbech-Jensen, Phys. Rev. B **53**, 14546 (1996).
[23] S. Matthias and F. Müller, Nature (London) **424**, 53 (2003).
[24] C. Mennerat-Robilliard *et al.*, Phys. Rev. Lett. **82**, 851 (1999).